Elsevier Editorial System(tm) for Composites Part B

Manuscript Draft

Manuscript Number: JCOMB-D-16-00516R1

Title: Influence of a Novel Organo-Silylated Clay on the Morphology, Thermal and Burning Behavior of Low Density Polyethylene Composites

Article Type: Full length article

Keywords: A. Nano structures; A. Polymer-matrix composites (PMCs); B. High-temperature properties; E. Thermoplastic resin; Burning behavior.

Corresponding Author: Prof. Paola Scarfato, Professor, PhD

Corresponding Author's Institution: University of Salerno

First Author: Paola Scarfato, Professor, PhD

Order of Authors: Paola Scarfato, Professor, PhD; Loredana Incarnato, Professor; Luciano Di Maio, Professor; Bettina Dittrich; Bernhard Schartel

Abstract: The functionalization of a natural sodium montmorillonite (MMT) with (3-glycidyloxypropyl)trimethoxysilane by a silylation procedure is presented, and its use as nanofiller in the melt compounding of low density polyethylene (LDPE) nanocomposites. In particular, the effects on the thermal stability and flame retardant properties of melt compounded LDPE nanocomposites are analyzed, with and without magnesium hydroxide (MH) as an additional conventional flame retardant. The purpose was to investigate possible synergistic effects between the two inorganic fillers on fire behavior. The obtained organosilylated clay showed higher interlayer spacing than the original MMT and good thermal stability, higher than that of many commercial organoclays modified with alkylammonium salts. Its addition to LDPE allowed the production of hybrids with nanoscale dispersion of the filler, as demonstrated by X-ray diffraction. The simultaneous presence of MH, which strongly interacts with the nanoclay, hindered intercalation of the polymer chains between the clay galleries and clay layer exfoliation within the LDPE resin.
The investigation of the thermal and burning behavior of the LDPE nanocomposites indicated that the organosilylated clay alone shows only a limited residual protection layer effect. In combination with MH the nanocomposites have a small adverse effect on the reaction to small flame as measured by the oxygen index and UL 94 testing, and, surprisingly, no effect on the peak heat release rate in the cone calorimeter. The quality of the fire residue was lacking on the microscopic scale. The ternary LDPE/MH/organoclay systems investigated did not open the door to reducing MH content in halogen-free flame retardant LDPE yet, but demand further research.

Università di Salerno
Dipartimento di Ingegneria Industriale

Fisciano, April 20, 2016

Dear Editor,

Thanks a lot for sending me your letter and the comments of the referees about the manuscript entitled "Influence of a Novel Organo-Silylated Clay on the Morphology, Thermal and Burning Behavior of Low Density Polyethylene Composites" (ref. no. JCOMB-D-16-00515) by myself et al. I reviewed the manuscript according to the revisions suggested by the referees. All the performed changes are detailed in the attached Detailed Response to Reviewers.

Sincerely,

Prof. Paola Scarfato

Department of Industrial Engineering - University of Salerno
Via Giovanni Paolo II, 132 - 84084 Fisciano (SA), Italy
Tel/fax: +39 089 963404
e-mail: pscarfato@unisa.it

***Detailed Response to Reviewers**

Fisciano, April 20, 2016

Manuscript "INFLUENCE OF A NOVEL ORGANO-SILYLATED CLAY ON THE MORPHOLOGY, THERMAL AND BURNING BEHAVIOR OF LOW DENSITY POLYETHYLENE COMPOSITES" (ref. no. **JCOMB-D-16-00515**) by P. Scarfato, L. Incarnato, L. Di Maio, B. Dittrich and B. Schartel.

<u>Detail of the performed changes:</u>

1. Page 6, Experimental Section, 2.3 Characterization paragraph.
   The sentence: "The d_{001} spacings of clays were calculated using Bragg's law." was replicated by: "The d_{001} spacings of clays were calculated from Bragg's law, i.e. $n\ \lambda = 2d \sin \theta$, where *n* is an integer and is equal to 1 for the first-order 001 x-ray reflection.", where the Bragg's law is reported.
2. Page 17, Results section, 3.5 Burning behavior paragraph.
   As pointed out by the referee, the sentence at the end of the page is not clear and it was rewritten as follows: "This leads to a burning behavior of LDPE/55MH and LDPE/60MH typical for charring, thermally thick materials [28]. In particular, compared to LDPE the typical main features of the changed burning behavior emerged. The PHRR at the end of burning nearly vanished and a strongly by 90% reduced PHRR occurred at the beginning of burning. The initial increase in HRR is followed by a more plateau-like HRR during combustion and accompanied by a prolonged burning time."

Prof. Paola Scarfato

Department of Industrial Engineering
University of Salerno
Via Giovanni Paolo II, 132 - 84084 Fisciano (SA), Italy
Tel: +39 089 963404 - e-mail: pscarfato@unisa.it

Influence of a Novel Organo-Silylated Clay on the Morphology, Thermal and Burning Behavior of Low Density Polyethylene Composites

Paola Scarfato[1,2], Loredana Incarnato[1], Luciano Di Maio[1], Bettina Dittrich[2], Bernhard Schartel[2]

[1]Department of Industrial Engineering, University of Salerno - Via Giovanni Paolo II 132, 84084 Fisciano (SA), Italy

[2]Bundesanstalt für Materialforschung und –prüfung (BAM) - Unter den Eichen 87, 12205 Berlin, Germany

Abstract

The functionalization of a natural sodium montmorillonite (MMT) with (3-glycidyloxypropyl)trimethoxysilane by a silylation procedure is presented, and its use as nanofiller in the melt compounding of low density polyethylene (LDPE) nanocomposites. In particular, the effects on the thermal stability and flame retardant properties of melt compounded LDPE nanocomposites are analyzed, with and without magnesium hydroxide (MH) as an additional conventional flame retardant. The purpose was to investigate possible synergistic effects between the two inorganic fillers on fire behavior. The obtained organosilylated clay showed higher interlayer spacing than the original MMT and good thermal stability, higher than that of many commercial organoclays modified with alkylammonium salts. Its addition to LDPE allowed the production of hybrids with nanoscale dispersion of the filler, as demonstrated by X-ray diffraction. The simultaneous presence of MH, which strongly interacts with the nanoclay, hindered intercalation of the polymer chains between the clay galleries and clay layer exfoliation within the LDPE resin.

The investigation of the thermal and burning behavior of the LDPE nanocomposites indicated that the organosilylated clay alone shows only a limited residual protection layer effect. In combination with MH the nanocomposites have a small adverse effect on the reaction to small flame as measured by the oxygen index and UL 94 testing, and, surprisingly, no effect on the peak heat release rate in the cone calorimeter. The quality of the fire residue was lacking on the microscopic scale. The ternary LDPE/MH/organoclay systems investigated did not open the door to reducing MH content in halogen-free flame retardant LDPE yet, but demand further research.

Keywords: A. Nano structures; A. Polymer-matrix composites (PMCs); B. High-temperature properties; E. Thermoplastic resin; Burning behavior.

1. Introduction

The improvement of relevant technological properties (mechanical, gas barrier, resistance to heat and flame, etc.) of polymeric matrices by the addition of layered organoclays, even at very low loading (<7-8 wt%), was demonstrated to be effective, particularly for several polar polymers (e.g. polyamides, polylactic acid, poly(ε-caprolactone), poly(methyl methacrylate), polyacrylonitrile, etc.) [1-10]. A good polymer-clay affinity favors the nanoscale dispersion of the organoclay and the delamination of the layered clay structure, thus leading to the formation of exfoliated morphologies responsible for enhanced performance. Remarkable synergistic effects of layered organoclays with other filler materials on reinforcement and on the flame retardancy of several matrices were also reported [11-15]. In particular, the combination of metal hydroxides with layered nanoparticles is one of the most successful approaches to reduce the filler amount needed to pass fire tests [16-21].

In the case of hydrophobic polymers such as polyethylene (PE), the advantages obtained have been limited up to now. Due to the poor adhesion between polymer and organoclay, generally only intercalated or poorly exfoliated morphologies are achieved, especially when the nanocomposites are produced by conventional melt intercalation techniques [22]. The results have remained largely unsatisfactory, even in the presence of compatibilizing and coupling agents. Barring the use of compatibilizer or coupling agents in excessive amounts, the question of how to obtain exfoliated structures in PE resins is still open and continues to attract many research efforts seeking the potential technological benefits that could ensue and lead to more advanced applications.

One possible strategy to increase the PE/nanoclay interactions, and thus to promote the compounding of nanocomposites, may be the use of layered clays functionalized with organosilane modifiers (R–Si-(OR′)$_3$). These agents are low in cost and react readily with the OH groups at the external surface, at the interlayer and at the edges of the clay mineral by condensation reactions, thus forming covalent bonds and yielding a decrease in the hydrophilicity of the clay surface and an increase in the distance between the layers [22-23]. Even though the use of silane coupling agents has been demonstrated to be effective in improving matrix/filler compatibility with several polymer systems, to the best of our knowledge this path has been explored only rarely in the scientific literature on developing PE/clay nanocomposites, in part because of the limited availability of commercial organosilylated clays [24].

In this study we successfully modified a natural sodium montmorillonite (MMT) with (3-glycidyloxypropyl)trimethoxysilane (GOPTMS) through a silylation procedure and used the obtained organosilylated layered clay as a nanofiller for a low density polyethylene (LDPE). LDPE nanocomposite systems at different loadings of organosilylated clay were produced by melt compounding using a pilot-scale twin-screw extruder, and characterized by several techniques in order to analyze the effects of the system's composition on the developed morphology, the thermal stability, the flammability and the burning behavior of the produced materials. Moreover, with the aim of investigating possible synergistic effects with conventional flame retardant additives, hybrid systems also containing magnesium hydroxide (MH) as an inorganic halogen-free flame retardant were also prepared and submitted to the same tests for comparison.

2. Experimental

2.1 Materials

The polymer matrix was an anhydride modified low density polyethylene (LDPE), (Tymax GT1057, M.I. = 7.5 g/10 min at 190°C/2.16 kg, 0.01 wt% of maleic anhydride grafted), supplied by Westlake Chemical.

The conventional flame retardant was magnesium hydroxide (MH) Magnifin H-5 A (Albemarle, Baton Rouge, LA, USA), with a particle size distribution of D50 = 1.4 – 2.0 microns.

The clay used as a nanofiller was a natural sodium montmorillonite (MMT) functionalized with (3-glycidyloxypropyl)trimethoxysilane (GOPTMS), the structure of which is shown in Figure 1. The MMT, with a specific surface area (N_2, BET) of 760 m^2/g and cationic exchange capacity (CEC) of 92 meq/100 g, was purchased from Altana-BYK. The GOPTMS (MW = 236.34 g/mol) was supplied by Sigma-Aldrich. All the other chemicals were of reagent grade and were used as received.

2.2 Preparation of organosilylated clay

The preparation of the organosilylated clay was performed according to the procedure reported by Chen et al. with a minor modification [25]. A calculated amount of organosilane was hydrolyzed for 4h at pH 3.0-4.0 in 200 mL of a solution of acetic acid in ethanol/deionized water mixture (90/10 wt/wt); the clay (10 g) was added and the mixture was then heated for 20 h with reflux at 50-90°C. The solution was diluted five times with ethanol to remove the soluble homocondensates, then was filtered, rinsed three times with 100 ml ethanol at room temperature and dried in a vacuum oven at 90°C for at least 48 h. The resulting product, referred below as SC1, was characterized by Fourier transform infrared spectroscopy, X-ray diffraction and thermogravimetric analyses in order to verify the effectiveness of the functionalization and to determine the clay interlayer spacing and the amount of silane grafting, as reported in the Results and Discussion section.

2.3 Processing

Hybrid LDPE-based systems with different percentages of SC1 and MH added were produced by melt compounding, using a twin-screw extruder (Dr. Collin GmbH - ZK 25–48D) with co-rotating intermeshing screws (D_{screw} = 25 mm, L/D = 42) and a volumetric feeder. A screw speed of 250 rpm and a temperature profile (from hopper to die) of 130-190-210-220-230°C were used. The strands of extruded materials were cooled in a water bath at approx. 15°C and a strand pelletizer (Dr. Collin GmbH CSG 171/2) used to produce pellets of suitable size for characterization. Before processing, all the materials were dried for 16 hours in oven under vacuum at 80°C, in order to prevent bubble formation and polymer degradation phenomena during extrusion. LDPE was processed under similar melt compounding conditions. The compositions of the investigated materials are listed in Table 1.

2.3 Characterization

X-ray diffraction (XRD) patterns were obtained by an automatic Bruker D8 Advance powder diffractometer, operated at 35 kV and 40 mA, in reflection mode, using nickel-filtered Cu Kα radiation (λ =1.5418 Å) at a scanning rate of 0.2 deg/min. The d_{001} spacings of clays were calculated from Bragg's law, i.e. $n \lambda = 2d \sin \theta$, where n is an integer and is equal to 1 for the first-order 001 x-ray reflection.

FT-IR measurements were carried out with a Nexus ThermoNicolet spectrometer equipped with a SmartPerformer accessory for attenuated total reflection (ATR) analysis. The spectra were collected on the samples in the frequency range 4000-400 cm^{-1} at 2 cm^{-1} spectral resolution and 64 scans were co-added.

The thermogravimetric analysis (TGA) of SC1 was carried out using a Shimadzu TGA-50 instrument to quantitatively determine the degree of grafting and yield as well as the thermal stability. The samples were heated from 40°C to 900°C at a heating rate of 20°C/min under nitrogen flow (50 ml/min).

The amount of grafted and intercalated aminosilanes was calculated using the following relationship [26].

Amount of grafted silane (meq/g)= $\frac{10^3 \times W_{200-600}}{[100-(W_{200-600})]\times M}$ eq. (1)

where $W_{200\text{-}600}$ corresponds to the mass loss between 200°C and 600°C and M (g/mol) is the molecular weight of the grafted silane molecules. The percentage that is grafted, which corresponds to the percentage of organic aminosilane moieties in the total inorganic mass, was calculated as follows:

Amount of grafted silane (%) = $\frac{100 \times W_{200-600}}{100 - W_{200-600}}$ eq. (2)

The TGA of LDPE and LDPE composites with SC1 and MH was measured on a Netzsch TG 209 ASC F1 Iris (Netzsch, Selb, Germany). Samples of approx. 10 mg in mass were heated from 30 to 900 °C in an inert atmosphere (nitrogen flow of 30 mL/min) with a heating rate of 10 °C/min.

Accelerated thermo-oxidative decomposition tests of the SC1 clay were carried out, exposing the samples incorporated in KBr disks for up to 8 h at 230°C in an air ventilated oven and evaluating the changes in their FT-IR spectrum over time.

Differential scanning calorimetry (DSC) measurements were performed with a Mettler DSC 822 calorimeter. The thermograms of 8 to 12 mg samples were obtained, sealed in standard aluminum pans, and the materials heated at 50°C/min from -50°C to 200°C under a nitrogen gas purge. The percentage of crystallinity (Xc) (corrected for filler content) was evaluated as the ratio of the melting enthalpy of the sample to the melting enthalpy of a 100% crystalline PE sample (293 J/g) [27].

The limiting oxygen index (LOI) was determined according to DIN EN ISO 4589-2 on bars of 125 mm × 6.5 mm × 3 mm, using an apparatus by Fire Testing Technology (FTT, East Grinstead, UK).

The UL 94 classification was determined by applying IEC 60695-11-10 to bars of 125 mm × 13 mm × 3 mm.

Investigation of the burning behavior under forced flaming conditions was carried out on a cone calorimeter by FTT according to ISO 5660. The samples 100 mm × 100 mm × 3 mm in size were irradiated with 50 kW/m^2 at a cone heater-specimen distance of 35 mm. Such a moderate distance delivers some advantages for measuring deforming materials without significantly changing the heat flux [28,29]. In particular, the area of constant heat flux and the reduction to the edges of the specimen are still similar to standard measurements at 25 mm distance. The materials were measured in duplicate when the results showed no deviation above 10% in any characteristic; otherwise three measurements were performed.

3. Results and Discussion

3.1 Characterization of SC1 clay

In order to verify that the layered sodium montmorillonite was successfully modified with (3-glycidyloxypropyl)trimethoxysilane and to fully characterize the starting material, the functionalized clay SC1 was submitted to XRD, FT-IR and TGA analyses. Figure 2 reports the XRD profile of SC1, together with that of the original MMT for comparison. The graph shows that the peak of SC1 was shifted to a smaller angle (2θ = 6.35 deg) than that of MMT (2θ = 9.15 deg), demonstrating that, under the experimental conditions chosen, the adopted organosilylation procedure produced an enlargement of the d_{001} interlayer spacing of the clay, which shifted from 0.97 nm to 1.39 nm.

The ATR FT-IR measurements confirm the organosilylation of the original clay, as is revealed in the spectra of MMT, SC1 and GOPTMS compared in Figure 3. Both the MMT and SC1 spectra are characterized by -OH absorption bands at ca. 3626 cm^{-1}, due to stretching vibrations of Al-OH and Si-OH, and at ca. 3440 cm^{-1} and 1640 cm^{-1}, due to stretching and bending vibrations of the interlayer water. The broadness of these signals is a consequence of the contributions of several structural -OH groups naturally occurring in the nanoclay. The strong signal at ca. 1040 cm^{-1} marks the stretching of Si-O groups, and the bands in the 600-400 cm-1 region show the bending vibrations of Si-O and Al-O. As regards the condensation reaction of the hydroxyl groups on the clay surface with the GOPTMS organosilane, the intensity of all these bands is lower in the modified clay. In addition, some new bands appear in the spectrum of SC1 clay, which belong to the organic part of organoclays: the CH_2 and CH_3 stretching vibrations at ca. 2925 cm^{-1} and 2883 cm^{-1}, respectively, and the C=O stretching at 1726 cm^{-1}, which can result from the opening reaction of the epoxy group of GOPTMS.

The TGA, the results of which are reported in Figure 4, allowed determination of the initial decomposition temperature (T_{onset}) of SC1, its temperature at the maximum rate of weight loss (DT_{max}), and the residual masses used to calculate the amount of grafted silane. The weight loss curve and the corresponding derivate curve show that SC1 displays two main decomposition intervals, one in the range of 200-600°C corresponding to the decomposition of the organosilane, the other in the range from 600°C to 900°C, corresponding to the dehydroxylation of aluminosilicate groups [30]. The T_{onset} was 320°C and the DT_{max} was 357°C; both values are significantly higher than those for most commercial montmorillonites modified with alkylammonium salts and are evidence for the high thermal stability of the SC1 organosilylated clay, which is crucial for its use in the melt compounding of many polymers (such as HDPE, nylon, TPU, etc.) requiring high processing temperatures, as well as for the nanocomposite properties and long term performance [30,31]. The amount of grafted organosilane, calculated according to eqs. 1 and 2, was 0.331 meq/g, corresponding to 7.82 wt%.

In order to assess the thermo-oxidative stability of the new SC1 clay, accelerated thermal decomposition tests were performed to expose it for different time intervals to 230°C, which is the highest temperature used in the processing of LDPE-based systems. The effects of the aging time (up to 8 h) on the ATR FT-IR spectrum of the sample are shown in Figure 5. The decrease in the -OH absorption bands (stretching at ca. 3454 cm^{-1} and bending at ca. 1640 cm^{-1}) indicates that the SC1 clay progressively loses the water contained in the interlayers, as expected. In contrast, the peaks due to the CH_2 and C=O stretching vibrations at around 2900-2800 cm^{-1} and 1729 cm^{-1} remain essentially unchanged after 8 h of thermal oxidation, indicating that the GOPTMS organic modifier is stable in the adopted aging conditions.

3.2 Characterization of LDPE-based systems

With the aim of obtaining information about the morphology developed during the process, all of the melt compounded LDPE-based systems with SC1 and MH added were submitted to XRD analysis.

Figure 6 compares the XRD profiles, in the range of low scattering angles, of SC1 organoclay and LDPE-based nanocomposites with different percentages of SC1 clay. The graph clearly shows that the original peak of SC1 is completely absent in the diffraction patterns of the LDPE/2SC1, LDPE/5SC1 and LDPE/8SC1 samples, demonstrating that the clay is dispersed on a nanometric scale in these systems. By contrast, the SC1 peak position remains almost unchanged in the LDPE-based hybrids that also contain MH at high loading levels (50 wt% and 55 wt%). It is proposed that MH, due to its hydrophilic nature, can establish stronger interactions through hydrogen bonding with SC1 than LDPE, thus promoting SC1 reaggregation and the output of the polymer chains from the clay galleries. It is well known, in fact, that the level of the interfacial interactions between the polymer and the nanofiller is a critical factor in determining the morphology and the equilibrium structure of a polymer/layered silicate nanocomposite system, as has been established in the literature [32-34]. In particular, theoretical and experimental studies have demonstrated that in the case of non-polar matrices like LDPE, the nanoscale dispersion of relatively polar clay lamellae is thermodynamically unstable; therefore, if the polymer is sufficiently fluid, the silicate layers tend to collapse as a result of the system melting [35].

All of the other small peaks in the XRD patterns of the LDPE/5SC1/50MH and LDPE/5SC1/55MH are related to MH.

Figure 7 compares the XRD profiles, in the scattering angle range from 10° to 40°, for all of the LDPE systems with different percentages of SC1 clay and MH. All of the patterns show the two principal crystalline reflections of interest in polyethylene at 2theta of 21.5° and 23.8°, corresponding to the 110 and 200 crystallographic lattice planes, respectively, and the amorphous halo centered at 2theta of ca. 19.8°. Moreover, the other strong peaks in the patterns of the hybrids containing MH at 2theta angles of 18.7° and 38.1° are related to the 001 and 101 crystallographic lattice planes of the mineral filler. It can be seen that the addition of increasing amounts of SC1 progressively decreases the crystallinity of the LDPE, indicating that the nanoclay acts as a barrier against crystal growth, as reported for several polymer/layered clay nanocomposite systems [36]. A further reduction in crystallinity was found in the hybrid systems incorporating high percentages of MH (above 50 wt%), without altering the crystal structure of the LDPE.

The lower degree of crystallinity in the filled samples compared to the neat LDPE was also confirmed by DSC measurements, as can be seen in Figure 8, which compares the heating thermograms and the thermal parameters of the LDPE, LDPE/5SC1 and LDPE/55MH samples, chosen as representative systems.

3.3 Pyrolysis

In order to investigate the effects of the SC1 and MH fillers on the thermal decomposition of the hybrid systems, TGA analyses in nitrogen atmosphere were carried out. The mass and mass loss rate are reported in Figure 9, and the onset temperature of decomposition (T_{onset}) and the temperature at maximum loss rate (DT_{max}), calculated from the mass loss rate curves, are listed in Table 2.

Figure 9 shows that in inert atmosphere the LDPE and the three LDPE/SC1 nanocomposites at different SC1 loadings decompose in a single step over a relatively short temperature range (ca. 450-500°C). The main decomposition pathways are random chain scission and branching, which occur simultaneously, yielding a single mass loss step [37]. The T_{onset} values remain essentially unchanged with the addition of the SC1 nanoclay, whereas the DT_{max} ones shift to slightly lower temperatures (DT = 4°C) for the nanocomposites at 5 wt% and 8 wt% of filler. Apart from the small increase in residue, in good approximation SC1 has no effect on the decomposition of LDPI. There is no stabilizing effect; if anything, the decomposition products enhanced the thermal decomposition of LDPE. The increase in residue corresponded to the amount of silicate incorporated.

In contrast, all of the hybrid systems containing MH in the formulation decompose in two merging steps. The first one corresponds to the decomposition of MH, the second one is due to the polymer. Taking into account the large filling grades and the overlapping with the preceding decomposition step of MH, the effects on T_{onset} (- 22°C) and DT_{max} (-6°C) are small for LDPE/55MH, LDPE/5SC1/50MH, and LDPE/60MH. Nevertheless, the decrease in T_{onset}, which amounts to -31°C for LDPE/5SC1/55MH, may indicate some limited predamage of the LPDE due to high shear rates during processing. There is interaction between MH and SC1, as the combination of the two fillers in the hybrid formulation shifts the T_{onset} and DT_{max} of MH towards higher temperatures. All composites containing MH showed a substantial increase in residue (37-43 wt%) due to the remaining MgO.

3.4 Reaction to small flame

In order to investigate the effects of the SC1 and MH fillers on the reaction to small flame of the LDPE-based hybrids, all of the systems were submitted to LOI and UL 94 tests. The results are reported in Table 3. As expected, the addition of MH causes the LOI to increase considerably, from 17.5 vol% for LDPE to 33.0 vol% for the LDPE/60MH, thanks to a combination of several flame retardancy modes of action [38,39]. The formation of a heat-shielding MgO layer on the sample surface reduces the heat flux from the flame to the underlying material and reduces the flow of combustible gases from the pyrolysis zone to the flame. The reaction from MH to MgO cools the condensed phase, since it is endothermic and goes along with the vaporization of water. The water vapor in the gas phase also cools the flame and dilutes the combustible LDPE decomposition products. Thus a higher percentage of oxygen is necessary to sustain the candle-like burning in the LOI test. The SC1 nanoparticles alone also increase the LOI values, but the change is very small. Actually, it may be still within the margin of uncertainty. The LOI value rises only from 17.5 up to 18.6 vol% for the LDPE/8SC1 system. The inorganic residue layer formed by the nanoclay on the surface is negligible protection against direct contact to a small flame applied in LOI and UL 94. The diminishing of flame retardancy effectiveness for low heat fluxes, and thus for LOI and UL 94, has been reported for several polymer/clay nanocomposites and was deduced as a general feature of nanocomposites in non-charring polymers [40-42]. The combined addition of SC1 and MH has an adverse effect on the LOI; at fixed MH content the LOI is lower when the SC1 clay is present in the formulation, demonstrating that no benefit was yielded by combining the flame retardant MH and the SC1 nanoclay during the burning of the LDPE-based hybrids.

At the filler loading levels considered in this work, neither MH nor SC1 yielded improvements in the UL 94 classification, which remained HB for all of the systems investigated.

3.5 Burning behavior

The burning behavior of LDPE with silylated clay SC1 and combinations of MH and SC1 under forced flaming conditions in the cone calorimeter are presented in Figure 10 and Table 4. LDPE presented a heat release rate (HRR) curve typical for thermally thin or intermediately thin non-charring materials, with a steady increase in HRR after ignition up to the peak HRR (PHRR) at the end of combustion [28]. The burning time was very short, the HRR pattern showed hardly any shoulder, and the PHRR with 2676 kW/m^2 was very high, all indicating thermally thin behavior. This interpretation of the HRR curve was confirmed by visual observation. The pyrolysis during burning involved nearly all LDPE material at once due to the complete melting of the polymer at the beginning of the test and the formation of a pool fire. The addition of 2 wt%, 5 wt% or 8 wt% of SC1 to LDPE decreased the time to ignition (TTI) with increasing filler content. In the literature, decreasing TTI has been reported for many layered silicate nanocomposites, and several reasons have been proposed to explain this phenomenon. In the investigated systems the surface catalysis of the oxidation of combustible volatiles and the reduction in convective heat transfer are two of the models proposed [43]. The latter phenomenon may be the most plausible, since it yields a consistent picture explaining both the earlier ignition and the somewhat hindered formation of the pool fire. The TTI of LDPE/SC1 nanocomposites decreased with increasing SC1 content by 9s (2 wt% filler), 15s (5 wt%), and 17s(8 wt%). The PHRR of LDPE/SC1 nanocomposites decreased with increasing SC1 content by 13% (2 wt% filler), 22% (5 wt%) and 32% (8 wt%), respectively. Despite the formation of residue agglomerates consisting of SC1, LDPE/SC1 composites still presented pool-like fire and non-charring burning behavior even with higher SC1 content. SC1 residue agglomerates were not able to adhere to each other and to form a stable protection layer on top of the sample plate due to the convection of molten LDPE and bubbles of volatiles bursting on the polymer surface (Figure 11a). This observation contrasts with what is usually known for analogous approaches, which yield successful, well-dispersed nanocomposites with layered silicates, carbon nanotubes or graphene materials. There, the increasing content of nanofillers hindered the movement of the polymer through increased melt viscosity, uniform and stable residues were obtained to work as a protection layer [8,40,44,45], and the reduction of PHRR was 50 up to 75% [8,40,41,46-48]. Thus both the measured reduction and visual observation indicated that the LDPE/SC1 nanocomposites did not exploit their full potential. One hypothesis to explain the limited reduction may be thermally induced agglomeration. For layered silicate/epoxy nanocomposites the opposite behavior was reported: better performance than expected based on delaminated but limited dispersed clay layers [50], and explained by the thermal decomposition of the matrix enabling exfoliation. The study proved that the timescale was short enough to change the state of exfoliation during pyrolysis. The nanodispersion at room temperature is only a prerequisite for the superior residue formation taking place during pyrolysis. For the LDPE/SC1 nanocomposites investigated, unfortunately, agglomeration induced by thermal decomposition can be proposed in the liquid state, caused by the decomposition of silane 120°C before the polymer decomposition. A second alternative explanation may be that the overall dispersion of the layers was not as good as assumed. Strictly speaking, the disappearance of the SC1 interlayer distance peak in the X-ray diffraction patterns in Figure 6 for LDPE/SC1 nanocomposites indicates the delamination of the clay layers, but not their exfoliation in terms of both delamination and dispersion. Actually, the intensity of the scattering angle between 2.5° and 4.5° may indicate such an inhomogeneous distribution over the specimen for LDEP/2SC1 and LDEP/5SC1. Due to an exclusive flame retardancy mechanism in the condensed phase by residue formation, with the addition of SC1 to LDPE the effective heat of combustion of volatiles – total heat evolved THE / total mass loss TML – remained constant at 4.4 MJ/m^2*g.

The HRR of MH-filled LDPE and SC1/MH-filled LDPE are shown in Figure 10b. The mineral filler MH in LDPE reacted to MgO and water vapor upon heating, the endothermic reaction led to a heat sink in the condensed phase, and the released water vapor cooled the gas phase and diluted the combustible volatile / oxygen mixture [38,39]. The time to reach ignition temperature increased from 49s for LDPE to 84s for LDPE/MH composites. The remaining MgO formed a residue layer shortly after ignition, reducing the incoming net heat flux to the pyrolysis front and decelerating specimen heating, polymer pyrolysis and volatile mass flow through its closed surface, stable structure and microscopically strong adhesion of agglomerates as seen in Figure 11b. This leads to a burning behavior of LDPE/55MH and LDPE/60MH typical for charring, thermally thick materials [28]. In particular, compared to LDPE the typical main features of the changed burning behavior emerged. The PHRR at the end of burning nearly vanished and a strongly by 90% reduced PHRR occurred at the beginning of burning. The initial increase in HRR is followed by a more plateau-like HRR during combustion and accompanied by a prolonged burning time. The fire load of the material is presented by the total heat evolved (THE), which is the integral of the heat release. In LDPE/MH composites, less combustible material is available due to the replacement of LDPE by MH, and thus the fire load of LDPE/55MH and LDPE/60MH was reduced compared to LDPE. The fire residue equaled the expected yield for MgO. The decrease in THE/TML from 4.4 MJ/m^2g for LDPE to 3.0 MJ/m^2g and 2.8 MJ/m^2g for LDPE/MH is a result of dilution by non-combustible water vapor release contributing to the mass loss, but not to the THE.

In LDPE/SC1/MH composites, MH was replaced by 5 wt% of organosilylated clay, resulting in the compositions LDPE/5SC1/50MH and LDPE/5SC1/55MH. The LDPE/SC1/MH composites behaved like charring, thermally thick materials similar to LDPE/MH composites. However, the overall HRR as well as the PHRR of LDPE/5SC1/50MH and LDPE/5SC1/55MH were slightly higher than for the corresponding LDPE/55MH and LDPE/60MH, respectively (Figure 10b). Actually the LDPE/5SC1/55MH shows very similar behavior to LDPE/55MH. Adding SC1 failed to add a significant flame retardancy effect. Regarding the surface of the fire residue, the macroscopic structure appeared more uniform, indicating an improvement of the protection layer through the replacement of MH by SC1 (Figure 11c). But on the microscopic scale, the MgO agglomerates in the residue appeared to be less adhered to each other, and the residue was also less stable and crumbly while handling. The fact that a deteriorated microscopic structure overcompensates for an improved macroscopic structure has been previously reported for the combination of layered silicate and ceepree glass [15]. Here, it was an unexpected result, as nanofillers – especially layered ones – are known to enhance the residue quality in many different systems, and particularly to improve burning behavior when combined with metal hydroxides [17-20,50]. In the case of the LDPE/SC1/MH composites, the interlayer distance peak of SC1 was observed in the XRD diffraction pattern. Therefore, the silicate layers of SC1 are supposed to remain in stacks, which results in insufficient particle dispersion of SC1 in the composite. The decreasing quality of the LDPE/SC1/MH fire residue structure reduced the protection layer efficiency of MH/SC1 and most probably led to the increase in HRR. By replacing 5 wt% MH with 5 wt% SC1, less water vapor from the thermal decomposition of MH was available to dilute the gas phase. So the effective heat of combustion increased, for example from 3.0 $MH/m^2 \cdot g$ for LDPE/55MH to 3.3 $MJ/m^2 \cdot g$ for LDPE/5SC1/50MH.

4. Conclusions

The study focused on the development of a new LDPE nanocomposite system produced by melt compounding of the polymer with three different percentages of a montmorillonite-based nanoclay, which was previously modified with (3-glycidyloxypropyl)trimethoxysilane. Based on the small angle x-ray diffractograms, the resulting hybrids are intercalated, exfoliated nanocomposites. Their potential in flame retardancy applications was investigated, analyzing their thermal stability, flammability and burning behavior, and the results compared with those for hybrid systems containing MH as an inorganic flame retardant, in order to check for possible synergistic effects between the silylated nanoclay and conventional flame retardant additives.

Although the organosilylated filler was dispersed on a nano-scale, it was demonstrated to be essentially ineffective in hindering the thermal decomposition of LDPE. Their flame retardancy effect is typical for nanocomposites with layered silicate, but less efficient than the flame retardancy reached in comparable systems. Moreover, the simultaneous presence of MH in the blends adversely affected the system morphology, promoting reaggregation of the organoclay layers. As a consequence, compared to the binary LDPE/MH systems, when replacing MH the ternary LDPE/MH/organoclay ones showed deterioration in the reaction to small flame and the quality of the protective fire residue.

Granting the systems investigated the freedom to behave as they wanted, this study obviously did not achieve its goals with respect to the fire performance achieved. The straightforward approach to combining layered silicate with metal hydroxide did not show the benefits it has in comparable systems. Thus this story teaches us how close to failure some of the successful nanocomposite systems proposed are, and how far away these nanotechnologies still are from becoming easy drop-in technologies.

References

1. Pinnavaia TJ, Beall G W, eds., Polymer-Layered Silicate Nanocomposites. New York: Wiley, 2001.
2. Sinha Ray S, Okamoto M. Polymer/layered silicate nanocomposites: a review from preparation to processing. Prog Polym Sci 2003;28:1539–1641.

3. Russo GM, Simon GP, Incarnato L. Correlation between Rheological, Mechanical, and Barrier Properties in New Copolyamide-Based Nanocomposite Films. Macromulecules 2006;39:3855–3864.
4. Di Maio L, Scarfato P, Milana MR, Feliciani R, Denaro M, Padula G, Incarnato L. Bionanocomposite Polylactic Acid/Organoclay Films: Functional Properties and Measurement of Total and Lactic Acid Specific Migration. Packag Technol Sci 2014;27:535-547.
5. Kojima Y, Usuki A, Kawasumi M, Okada A, Fukushima Y, Karauchi T, Kamigaito OJ. Synthesis of nylon 6–clay hybrid by montmorillonite intercalated with ϵ-caprolactam. J Polym Sci A Polym Chem 1993;31:983–986.
6. Gilman JW. Flammability and thermal stability studies of polymer layered-silicate (clay) nanocomposites. Appl. Clay Sci. 1999;15:31–49.
7. Zanetti M, Camino G, Mülhaupt R. Combustion behaviour of EVA/fluorohectorite nanocomposites. Polym Degrad Stab 2001;74:413–417.
8. Kashiwagi T, Harris RH Jr, Zhang X, Briber RM, Cipriano B H, S R Raghavan, Awad W H, Shields J R. Flame retardant mechanism of polyamide 6–clay nanocomposites. Polymer 2004;45(3):881-891.
9. Di Maio L, Garofalo E, Scarfato P, Incarnato L. Effect of polymer/organoclay composition on morphology and rheological properties of polylactide nanocomposites. Polym Composite 2015;36(6):1135-1144.
10. Uddin Md E, Kanta Layek R, Hoon Kim N, Hui D, Hee Lee J. Preparation and properties of reduced graphene oxide/polyacrylonitrile nanocomposites using polyvinyl phenol. Compos Part B Eng 2015;80:238-245.

11. Montero B, Bellas R, Ramírez C, Rico M, Bouza R. Flame retardancy and thermal stability of organic–inorganic hybrid resins based on polyhedral oligomeric silsesquioxanes and montmorillonite clay. Compos Part B Eng 2014;63:67-76.
12. Tang C, Xiang L, Su J, Wang K, Yang C, Zhang Q, Fu Q. Largely improved tensile properties of chitosan film via unique synergistic reinforcing effect of carbon nanotube and clay. J Phys Chem B 2008;112:3876-3881.
13. Peeterbroeck S, Alexandre M, Nagy JB, Pirlot C, Fonseca A, Moreau N, Philippin G, Delhalle J, Mekhalif Z, Sporken R, Beyer G, Dubois P. Polymer-layered silicate -carbon nanotube nanocomposites: Unique nanofiller synergistic effect. Compos Sci Technol 2004;64(15):2317-2323.
14. Chigwada G, Jash P, Jiang DD, Wilkie CA. Fire retardancy of vinyl ester nanocomposites: Synergy with phosphorus-based fire retardants. Polym Degrad Stab 2005;89:85-100.
15. Bee S-T, Hassan A, Ratnam CT, Tee T-T, Tin Sin L, Hui D. Dispersion and roles of montmorillonite on structural, flammability, thermal and mechanical behaviours of electron beam irradiated flame retarded nanocomposite. Compos Part B Eng 2014;61:41-48.
16. Wu G M, Schartel B, Kleemeier M, Hartwig A. Flammability of layered silicate epoxy nanocomposites combined with low-melting inorganic ceepree glass. Polym Eng Sci 2012;52:507-517.
17. Beyer G. Flame retardant properties of EVA-nanocomposites and improvements by combination of nanofillers with aluminium trihydrate. Fire Mater 2001;25(5):193-197.

18. Beyer G. Filler blend of carbon nanotubes and organoclays with improved char as a new flame retardant system for polymers and cable applications. Fire Mater 2005;29:61-69.
19. Schartel B, Knoll U, Hartwig A, Pütz D. Phosphonium-Modified Layered Silicate Epoxy Resins Nanocomposites and their Combinations with ATH and Organo-Phosphorus Fire Retardants. Polymer Adv Tech 2006;17:281-293.
20. Dittrich B, Wartig K-A, Mülhaupt R, Schartel B. Flame-Retardancy Properties of Intumescent Ammonium Poly(Phosphate) and Mineral Filler Magnesium Hydroxide in Combination with Graphene. Polymers 2014;6:2875-2895.
21. Gallo E, Schartel B, Acierno D, Russo P. Flame retardant biocomposites: Synergism between phosphinate and nanometric metal oxides. Eur Polym J 2011;47(7):1390-1401.
22. Chrissafis K, Paraskevopoulos K M, Tsiaoussis I, Bikiaris D. Comparative study of the effect of different nanoparticles on the mechanical properties, permeability, and thermal degradation mechanism of HDPE. J Appl Polym Sci 2009;114:1606–1618.
23. Kango S, Kalia S, Celli A, Njugun J, Habibi Y, Kumar R. Surface modification of inorganic nanoparticles for development of organic-inorganic nanocomposites: A review. Prog Polym Sci 2013;38:1232-1261.
24. Betega de Paiva L, Morales AR, Valenzuela Díaz FR. Organoclays: Properties, preparation and applications. Appl Clay Sci 2008;42:8–24.
25. Chen GX, Kim HS, Shim JH, Yoon J-S. Role of epoxy groups on clay surface in the improvement of morphology of poly(l-lactide)/clay composites. Macromolecules 2005;38:3738-3744.

26. Negrete-Herrera N, Letoffe JM, Puteaux JL, David L, Bourgeat-Lami E. Aqueous dispersions of silane-functionalized laponite clay platelets. A first step toward the elaboration of water-based polymer/clay nanocomposites. Langmuir 2004;20:1564-1571.
27. Peacock AJ. *Handbook of Polyethylene: Structures: Properties, and Applications.* New York: Marcel Dekker, 2000. 177.
28. Schartel B, Hull TR. Development of fire-retarded materials: Interpretation of cone calorimeter data. Fire Mater 2007;31(5):327-354.
29. Schartel B, Bartholmai M, Knoll U. Some comments on the use of cone calorimeter data. Polym Degrad Stab 2005;88(3):540-547.
30. Xie W, Gao ZM, Pan WP, Hunter D, Singh A, Vaia R. Thermal degradation chemistry of alkyl quaternary ammonium montmorillonite. Chem Mater. 2001;13:2979-2990.
31. Cervantes-Uc JM, Cauich-Rodríguez JV, Vázquez-Torres H, Garfias-Mesías LF, Paul DR. Thermal degradation of commercially available organoclays studied by TGA–FTIR. Thermochim Acta 2007;457:92-102.
32. Sinha Ray S, Okamoto M. Polymer/layered silicate nanocomposites: A review from preparation to processing. Prog Polym Sci 2003;28:1539–1641.
33. Ganesan V, Jayaraman A. Theory and simulation studies of effective interactions, phase behavior and morphology in polymer nanocomposites. Soft Matter 2014;10:13-38.
34. Vaia RA, Giannelis EP. Lattice Model of Polymer Melt Intercalation in Organically-Modified Layered Silicates. Macromolecules 1997;30:7990-7999.

35. Alexandre M, Dubois P, Sun T, Garces JM, Jérôme R. Polyethylene-layered silicate nanocomposites prepared by the polymerization-filling technique: Synthesis and mechanical properties. Polymer 2002;43:2123-2132.
36. Sinha Ray S. Environmentally Friendly Polymer Nanocomposites: Types, Processing and Properties. Cambridge (UK): Woodhead Publishing, 2013.
37. Hinsken H, Moss S, Pauquet J-R, Zweifel H. Degradation of polyolefins during melt processing. Polym Degrad Stab 1991;34:279–293.
38. Horn WE. In: Grand AF, Wilkie CA, eds. Fire Retardancy of Polymeric Materials. New York: Marcel Dekker, 2000. 285–352.
39. Rothon RN, Hornsby PR. Flame retardant effects of magnesium hydroxide. Polym Degrad Stab 1996;54(2-3):383-385.
40. Schartel B, Bartholmai M, Knoll U. Some comments on the main fire retardancy mechanisms in polymer nanocomposites. Polym Adv Technol 2006;17(9-10):772-777.
41. Bartholmai M, Schartel B, Layered silicate polymer nanocomposites: new approach or illusion for fire retardancy? Investigations of the potentials and the tasks using a model system. Polym Adv Technol 2004;15(7):355-364.
42. Hartwig A, Pütz D, Schartel B, Bartholmai M, Wendschuh-Josties, M. Combustion behaviour of epoxide based nanocomposites with ammonium and phosphonium bentonites. Macromol Chem Physic 2003;204:2247-2257.
43. Fina A, Camino G. Ignition mechanisms in polymers and polymer nanocomposites. Polym Adv Technol 2011;22(7):1147-1155.

44. Wu GM, Schartel B, Bahr H, Kleemeier M, Yu D, Hartwig A. Experimental and quantitative assessment of flame retardancy by the shielding effect in layered silicate epoxy nanocomposites. Combust Flame 2012;159:3616-3623.
45. Schartel B, Weiß A. Temperature inside burning polymer specimens: pyrolysis zone and shielding. Fire Mater 2010;34:217-235.
46. Dittrich B, Wartig K-A, Hofmann D, Mülhaupt R, Schartel B. The influence of layered, spherical, and tubular carbon nanomaterials' concentration on the flame retardancy of polypropylene. Polym Composite 2015;36:1230-1241.
47. Kashiwagi T, Fagan J, Douglas JF, Yamamoto K, Heckert A N, Leigh S D, Obrzut J, Du F, Lin-Gibson S, Mu M, Winey KI, Haggenmueller R. Relationship between dispersion metric and properties of PMMA/SWNT nanocomposites. Polymer, 2007;48(16):4855-4866.
48. Kashiwagi T, Du F, Winey K I, Groth K M, Shields J R, Bellayer S P, Kim H, Douglas J F. Flammability properties of polymer nanocomposites with single-walled carbon nanotubes: Effects of nanotube dispersion and concentration. Polymer 2005;46(2):471-481.
49. Schartel B, Weiß A, Sturm H, Kleemeier M, Hartwig A, Vogt C, Fischer R X. Layered silicate epoxy nanocomposites: formation of the inorganic-carbonaceous fire protection layer. Polym Adv Technol 2011;22:1581-1592.
50. Morgan AB. Flame retarded polymer layered silicate nanocomposites: A review of commercial and open literature systems. Polym Adv Technol 2006;17(4):206-217.

List of Tables

List of Figures

Figure 8. DSC heating thermograms and corresponding thermal parameters of neat LDPE, LDPE/5SC1 and LDPE/55MH samples.

Figure 9. Weight curves (a) and mass loss rate (b) of the LDPE-based systems at different percentages of SC1 and magnesium hydroxide (MH).

Figure 10. Burning behavior of the LDPE-based systems with (a) different percentages of SC1 organosilylated clay added and (b) with magnesium hydroxide (MH)/SC1 combinations.

Figure 11. Fire residue structure of the surface and microscopic structure of a) LDPE/8SC1, b) LDPE/55MH and c) LDPE/5SC1/50MH.

Table

Table 1. Composition of the investigated LDPE-based systems with SC1 (organosilylated clay) and MH (magnesium hydroxide) added.

Sample	*LDPE (wt%)*	*SC1 (wt%)*	*MH (wt%)*
LDPE	100	-	-
LDPE/2SC1	98	2	-
LDPE/5SC1	95	5	-
LDPE/8SC1	92	8	-
LDPE/55MH	45	-	55
LDPE/60MH	40	-	60
LDPE/5SC1/50MH	47.5	2.5	50
LDPE/5SC1/55MH	42.75	2.25	55

Table 2. Initial degradation temperatures (T_{onset}), temperatures of maximum rate of weight loss (DT_{max}), mass loss (ML) at the transition of both steps and residue at 800 °C of the LDPE and of LDPE/SC1 nanocomposites at different percentages of SC1 clay and magnesium hydroxide (MH).

	Sample	*LDPE*	*LDPE/ 2SC1*	*LDPE/ 5SC1*	*LDPE/ 8SC1*	*LDPE/ 55MH*	*LDPE/ 60MH*	*LDPE/ 5SC1/50MH*	*LDPE/ 5SC1/55MH*
Pre-step	**T_{onset} (°C)**					362	362	371	366
	DT_{max} (°C)					402	400	418	412
Main step	**T_{onset} (°C)**	454	454	453	454	435	433	429	423
	DT_{max} (°C)	477	476	473	474	471	472	470	463
	Residue (wt%)	0	1.5	3.7	5.9	39.4	42.8	36.8	39.6

Table 3. Limiting oxygen index (LOI) for the LDPE-based systems with different percentages of SC1 organosilylated clay and magnesium hydroxide (MH) added.

Sample	*LDPE*	*LDPE/ 2SC1*	*LDPE/ 5SC1*	*LDPE/ 8SC1*	*LDPE/ 55MH*	*LDPE/ 60MH*	*LDPE/ 5SC1/55MH*	*LDPE/ 5SC1/50MH*
LOI (vol%)	17.5	18.3	18.3	18.6	31.9	33.0	29.3	28.6
UL 94	HB	HB	HB	HB	HB	HB	HB	HB

Table 4. Cone calorimeter (50 kW/m^2) burning behavior data of LDPE, LDPE/SC1, LDPE/MH and LDPE/MH/SC1 composites

Sample	*LDPE*	*LDPE/ 2SC1*	*LDPE/ 5SC1*	*LDPE/ 8SC1*	*LDPE/ 55MH*	*LDPE/ 60MH*	*LDPE/ 5SC1/55MH*	*LDPE/ 5SC1/50MH*
TTI (s)	49	40	34	32	84	84	62	74
PHRR (kW/m^2)	2672±107	2324±336	2089±215	1825±80	261±10	237±9	304±16	258±10
Red_{PHRR} (%)		13	22	32	90	91	89	90
THE (MJ/m^2)	113 ± 5	117 ± 5	112 ± 5	113 ± 5	78 ± 3	70 ± 3	86 ± 5	76 ± 3
Red_{THE} (%)		0	0	0	31	38	24	33
$Residue_{exp}$ (wt%)±1.0	0	1.4	3	5	38.3	41.9	36.6	40.5
THE/TML (MJ/(m^2g))	4.4	4.4	4.3	4.3	3.0	2.8	3.3	3.0
TTI (s)	49	40	34	32	84	84	62	74

Figure 1

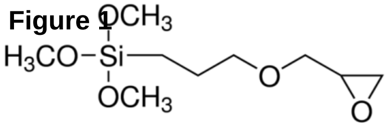

Figure 2

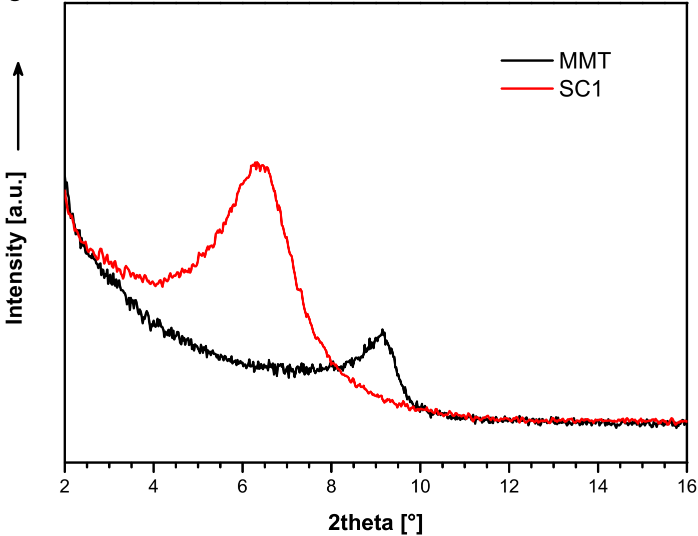

Figure 3

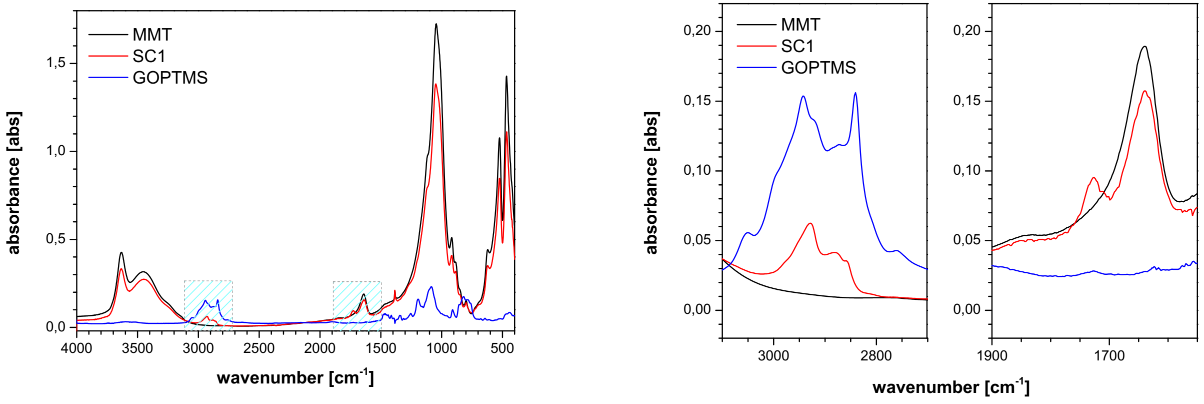
MMT
SC1
GOPTMS
absorbance [abs]
wavenumber [cm-1]
1,5
1,0
0,5
0,0
4000
3500
3000
2500
2000
1500
1000
500
0,20
0,15
0,10
0,05
0,00
3000
2800
1900
1700

(a)

(b)

Figure 4

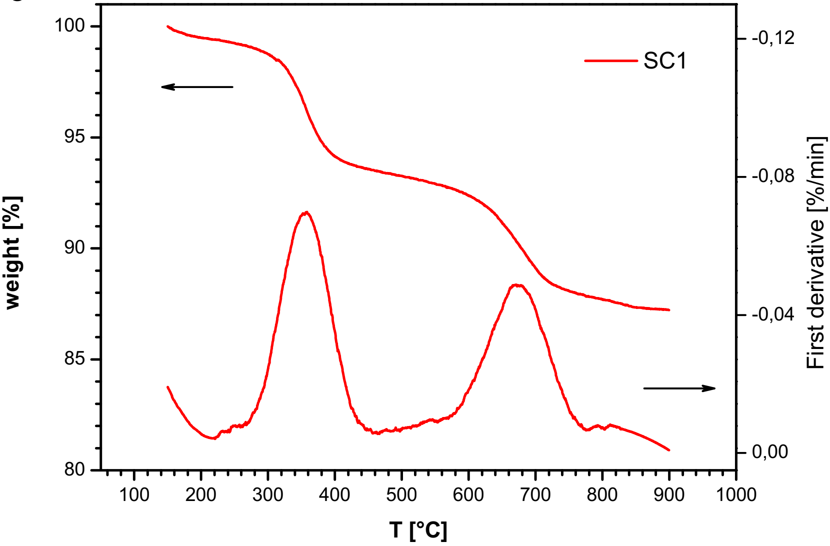

SC1
weight [%]
First derivative [%/min]
T [°C]
100
95
90
85
80
-0,12
-0,08
-0,04
0,00
100
200
300
400
500
600
700
800
900
1000

Figure 5

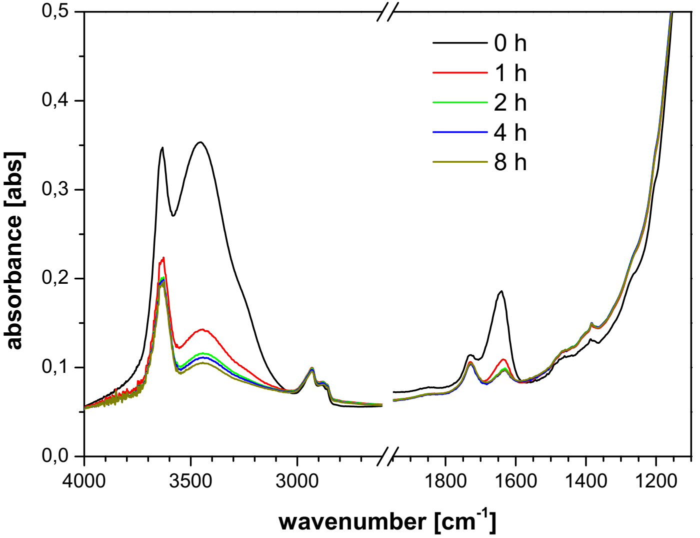

0 h
1 h
2 h
4 h
8 h
absorbance [abs]
0,0
0,1
0,2
0,3
0,4
0,5
4000
3500
3000
1800
1600
1400
1200
wavenumber [cm-1]

Figure 6

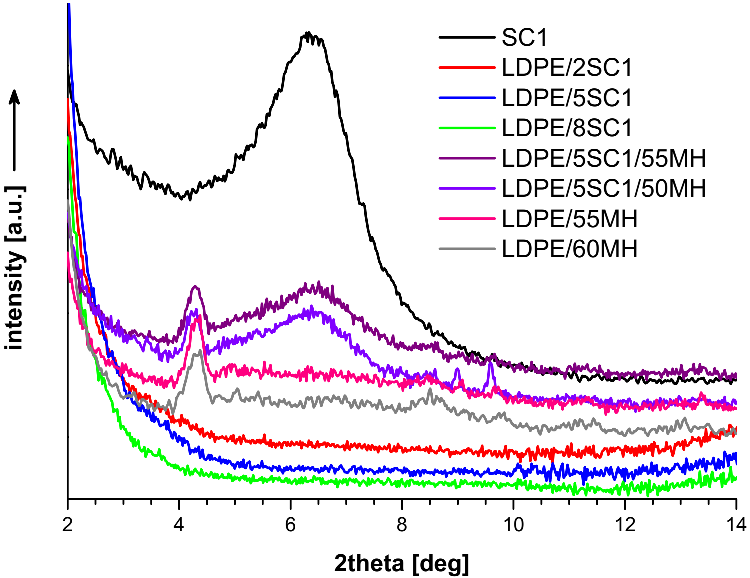

SC1
LDPE/2SC1
LDPE/5SC1
LDPE/8SC1
LDPE/5SC1/55MH
LDPE/5SC1/50MH
LDPE/55MH
LDPE/60MH
intensity [a.u.]
2theta [deg]
2
4
6
8
10
12
14

Figure 7

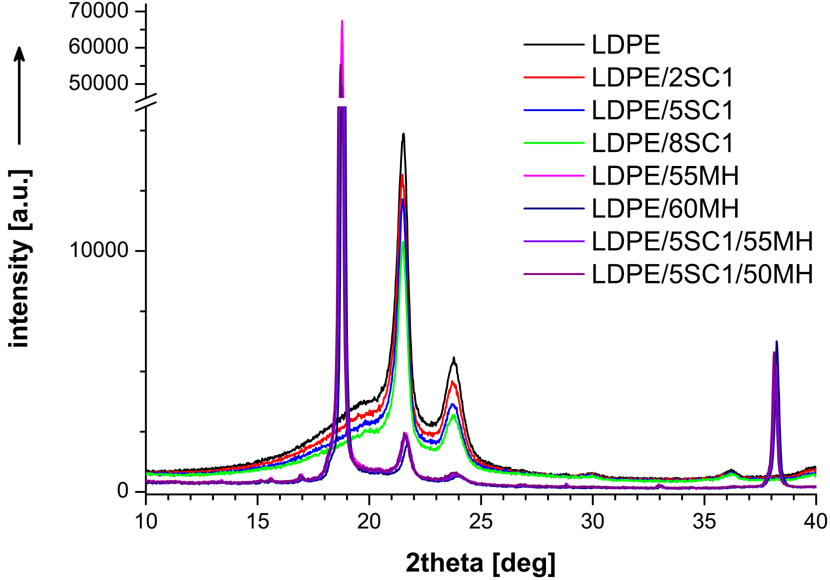

70000
60000
50000
10000
0
10
15
20
25
30
35
40
intensity [a.u.]
2theta [deg]
LDPE
LDPE/2SC1
LDPE/5SC1
LDPE/8SC1
LDPE/55MH
LDPE/60MH
LDPE/5SC1/55MH
LDPE/5SC1/50MH

Figure 8

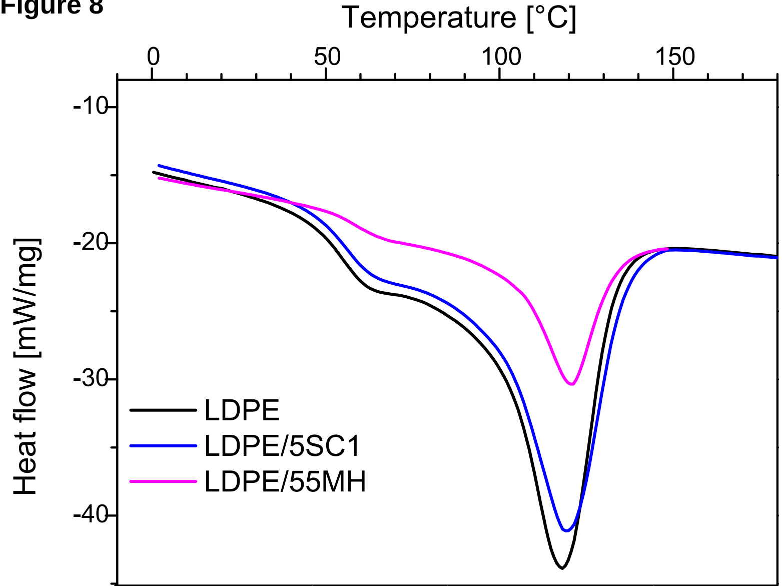

	T*m* [°C]	ΔH*m* [J/g]	X*c* [%]
LDPE	118	-120	41
LDPE/5SC1	119	-107	38
LDPE/55MH	120	-42	32

Figure 9

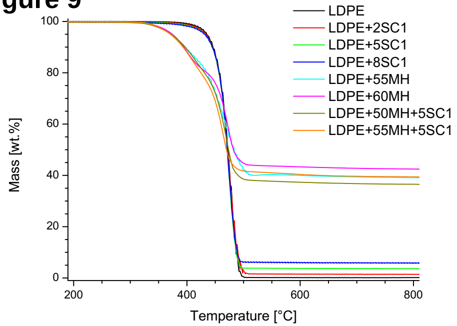
LDPE
LDPE+2SC1
LDPE+5SC1
LDPE+8SC1
LDPE+55MH
LDPE+60MH
LDPE+50MH+5SC1
LDPE+55MH+5SC1
Mass [wt.%]
Temperature [°C]
100
80
60
40
20
0
200
400
600
800

(a)

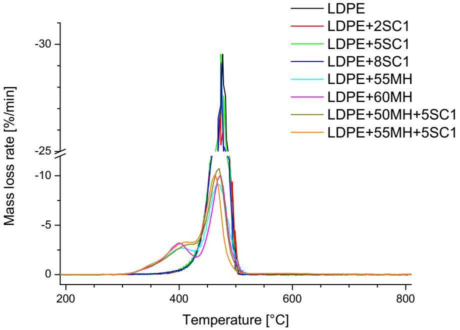
LDPE
LDPE+2SC1
LDPE+5SC1
LDPE+8SC1
LDPE+55MH
LDPE+60MH
LDPE+50MH+5SC1
LDPE+55MH+5SC1
Mass loss rate [%/min]
Temperature [°C]
-30
-25
-10
-5
0
200
400
600
800

(b)

Figure 10

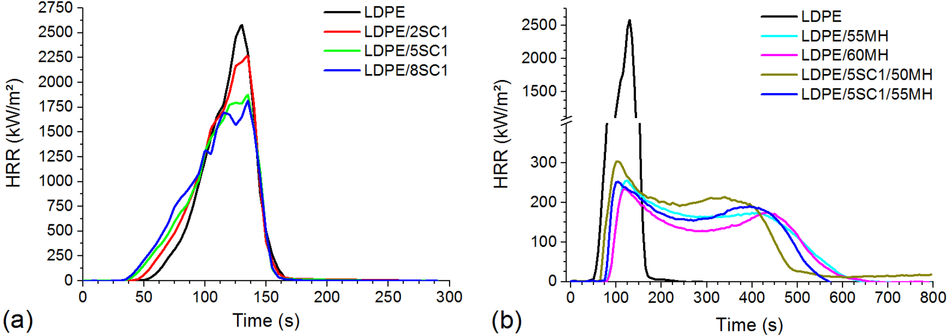

HRR (kW/m²)
Time (s)
LDPE
LDPE/2SC1
LDPE/5SC1
LDPE/8SC1
(a)
LDPE
LDPE/55MH
LDPE/60MH
LDPE/5SC1/50MH
LDPE/5SC1/55MH
(b)

Figure 11